

The Coulomb problem in iron based superconductors

Elio J. König¹ and Piers Coleman^{1,2}

¹*Department of Physics and Astronomy, Rutgers University, Piscataway, New Jersey, 08854, USA*

²*Department of Physics, Royal Holloway, University of London, Egham, Surrey TW20 0EX, UK*

(Dated: April 18, 2019)

We discuss the role of strong Coulomb interactions in iron-based superconductors (FeSCs). The presumed s^\pm character of these superconductors means that the condensate is not symmetry protected against Coulomb repulsion. Remarkably, the transition temperatures and the excitation gap are quite robust across the large family of iron based superconductors, despite drastic changes in Fermi surface geometry. The Coulomb problem is to understand how these superconductors avoid the strong onsite Coulomb interaction at the iron atoms, while maintaining a robust transition temperature. Within the dominant space of t_{2g} orbitals, on-site repulsion in the FeSCs enforces two linearly independent components of the condensate to vanish. This raises the possibility that iron-based superconductors might adapt their condensate to the Coulomb constraints by rotating the pairing state within the large manifold of entangled, extended s-wave gap functions with different orbital and momentum space structure. We examine this “orbital and k-space flexibility” (OKF) mechanism using both Landau theory and microscopic calculations within a multi-orbital t-J model. Based on our results, we conclude that OKF necessitates a large condensate degeneracy. One interesting possibility raised by our results, is that a resolution to the Coulomb problem in FeSC might require a reconsideration of triplet pairing.

PACS numbers: 74.20.Rp, 74.70.Xa

I. INTRODUCTION

Ten years after their discovery [1], iron based superconductors (FeSC) remain at the focus of condensed matter research. These materials offer great promise for applications, providing robust high temperature superconductivity at high current densities and magnetic fields. On the other hand, from a fundamental physics perspective, the rich phase diagram and the unresolved pairing mechanism of the iron-based superconductors continue to attract both experimental and theoretical attention.

Discoveries over the past decade have revealed a broad family of iron-based superconductors. Generally, they are categorized by their chemical compositions, and the most prominent classes are the 1111, 122, 111, and 11 families. All iron-based superconductors share a common local electronic structure, with the iron atoms contained within a tetrahedron of pnictide or chalcogenide atoms. These tetrahedra are closely packed in a staggered formation with two iron atoms per unit cell, forming a two dimensional layered structure. There are two slight exceptions: the quasi-1D compound BaFe_2S_3 [2, 3] in which the paired tetrahedra form two-leg ladders of iron atoms, and single layer FeSe [4]. By contrast, the momentum-space electronic structures of the FeSC show great diversity, see Table I. Many of the layered materials display both hole and electron pockets, respectively located at the Γ and X points of the Brillouin zone. However, KFe_2As_2 only has hole pockets centered at the Γ point [5, 6], while in various iron chalcogenides there are only electron pockets [7]. There is no indication for a clear trend in the transition temperatures as pockets disappear. At the same time, a universal $2\Delta_{\text{max}}/k_B T_c \approx 7.2$ suggests a common mechanism for superconductivity in all FeSC [8].

The Fermi surfaces of the FeSC are primarily composed from the t_{2g} orbitals of the iron d -shell. The electron correlations increase from the 1111 to 122 and 111 compounds,

and are maximal in the 11 materials. First principle calculations [9] indicate that the intra orbital and inter orbital on-site Coulomb energies, denoted by U and U' , are about 5 to 15 times larger than the hopping matrix elements, which are comparable to the Hund’s coupling J_H . Evidence for Hubbard-like side bands [10, 11], were reported very recently, however, the vast majority of FeSC do not display a Mott phase. The strong interaction energies on the one hand, and the experimentally observed metallicity on the other hand have catalyzed two opposing theoretical view points, which focus on “local” [12, 13] and “itinerant” [14, 15] aspects of the physics.

Based on Knight shift experiments, the superconducting gap structure [16] of iron based superconductors is believed to be spin-singlet in character. While many materials show a full gap, there is some indirect experimental support for condensate pairing amplitudes with opposite signs on different Fermi surfaces [17]. Recent experiments have underlined the importance of orbital selective physics, both in the normal state [18, 19] and in the superconducting state [20].

A. The Coulomb Problem

Despite the enormous progress of the past years, two unsolved questions about the pairing mechanism in the iron-based superconductors stand out:

- Why does superconductivity appear so generically, independently of very different Fermi surface topologies?
- What is the common mechanism by which FeSC overcomes the strong Coulomb repulsion at the iron sites?

In almost all other strongly correlated pair condensates including the cuprate superconductors, Sr_2RuO_4 , heavy fermion and organic superconductors, and superfluid ^3He , the condensate

avoids the local repulsion by forming finite angular momentum Cooper pairs. This is because the nodes in the finite an-

gular momentum Cooper pairs guarantee a vanishing on-site component of the pair expectation value, thereby protecting the condensate against large Coulomb repulsion.

In an orbital basis, the onsite Coulomb interaction is written

$$\hat{V}_C = \frac{1}{2} \sum_{j, m_i, \alpha, \beta} (m_1, m_2 | \hat{V} | m'_1, m'_2) \psi_{m_1 \alpha}^\dagger(\mathbf{x}_j) \psi_{m_2 \beta}^\dagger(\mathbf{x}_j) \psi_{m'_2 \beta}(\mathbf{x}_j) \psi_{m'_1 \alpha}(\mathbf{x}_j), \quad (1)$$

$\psi_{m, \alpha}^\dagger(\mathbf{x}_j)$ creates an electron in orbital m , spin component $\alpha \in \{\uparrow, \downarrow\}$ at position \mathbf{x}_j and

$$(m_1, m_2 | \hat{V} | m'_1, m'_2) = \int d^3x d^3y V_c(\mathbf{x} - \mathbf{y}) \phi_{m_1}(\mathbf{x}) \phi_{m'_1}(\mathbf{x}) \phi_{m_2}(\mathbf{y}) \phi_{m'_2}(\mathbf{y}) \quad (2)$$

is the integral of the Coulomb interaction $V_c(\mathbf{x} - \mathbf{y})$ with the atomic orbitals, $\phi_m(\mathbf{x})$. In an isotropic environment, a simplified version of the interaction can be written[21]

$$\hat{V} = \frac{U}{2} \sum_j n_j^2 - J_{H,1} \sum_j \tilde{S}_j^2 - J_{H,2} \sum_j \tilde{L}_j^2 \quad (3)$$

where $n_j = \sum_{m, \alpha} \psi_{m \alpha}^\dagger(\mathbf{x}_j) \psi_{m \alpha}(\mathbf{x}_j)$ is the number of d-electrons at site j , while \tilde{S}_j and \tilde{L}_j are the corresponding total spin and orbital angular momentum at site j , respectively. The leading Coulomb repulsive U is of order 2-4eV, while the subleading Hund's interactions, $J_{H,1}$ and $J_{H,2}$ are typically a few tenths of eV [9]. These large interactions are certainly not unique to the iron-based superconductors: they feature in almost all iron-based compounds and they drive a wide variety of both Mott and Hund's physics, such as the ferromagnetism in iron, which develops at the astonishingly high temperature of 1043K, and the Mott insulating behavior of rust (Fe_2O_3).

The important point is that in the iron-based superconductors, the characteristic gap energies on the scale of tens of millivolts, are dwarfed by the onsite Coulomb interactions on the scale of volts. Once a superconducting condensate forms, the additional onsite charge fluctuations associated with the coherent state modify the Coulomb energy. The key quantity determining this condensate correction to the Coulomb energy is the anomalous equal-time Gor'kov function

$$\langle \psi_{m \alpha}(\mathbf{x}_j) \psi_{m' \beta}(\mathbf{x}_j) \rangle = \epsilon_{\alpha \beta} F_{m m'}.$$

Here we have restricted ourselves to spin-singlet pairing, in which the Gor'kov function is proportional to the antisymmetric tensor $\epsilon_{\alpha \beta} = -\epsilon_{\beta \alpha}$. If we evaluate the change in the condensation energy in the Hartree Fock approximation, by contracting the anomalous terms in the energy, then for the isotropic interaction the change in condensate energy per site is

$$\begin{aligned} \Delta E &= \frac{1}{N_s} \left[\langle \psi_{SC} | \hat{V} | \psi_{SC} \rangle - \langle \psi_{FL} | \hat{V} | \psi_{FL} \rangle \right] \\ &= \sum_{m, m'} |F_{m, m'}|^2 [\tilde{U} + 2J_{H,2} \delta_{m, m'}], \end{aligned} \quad (4)$$

where N_s is the number of sites, and $|\Psi_{SC}\rangle$ ($|\Psi_{FL}\rangle$) is the superconducting (Fermi liquid) many body ground state. Here, the Coulomb cost is $\tilde{U} = U + (3J_{H,1} - 4J_{H,2})/2$, to be specific we have considered the case of a t_{2g} triplet ($m \in \{zx, zy, xy\}$). The huge discrepancy of scale between the Coulomb and gap energies, means that for the stabilization

of the condensate, the onsite pairing terms have to vanish, i.e

$$F_{m, m'} = \frac{1}{2} \epsilon_{\beta \alpha} \langle \psi_{m \alpha}(\mathbf{x}_j) \psi_{m' \beta}(\mathbf{x}_j) \rangle = 0. \quad (5)$$

These are the Coulomb constraints on the condensate.

If we rewrite the Coulomb constraint in the momentum and frequency domain it becomes

$$F_{m, m'} = \int \frac{d^3k}{(2\pi)^3} \frac{d\omega}{\pi} f(\omega) \text{Im}[F_{m, m'}(\mathbf{k}, \omega - i\delta)] = 0, \quad (6)$$

where $f(\omega) = (\exp[\beta\omega] + 1)^{-1}$ is the Fermi function. Typically, the integrand in Eq. (6) is dominated by the Fermi surfaces and is quite sensitive to the electronic structure. In d-wave superconductors, such as the heavy fermion and cuprate superconductors, satisfaction of the Coulomb constraint is symmetry-protected, because the alternating signs of the four quadrants of the gap function cause the momentum summation to automatically vanish. However, for s-wave superconductors the Coulomb constraint is unprotected by symmetry. In many of the early iron-based superconductors the Coulomb constraint was thought to be satisfied by dint of the s_{\pm} character, with alternating gap signs on the electron and hole pockets. However, the subsequent discovery that iron-based superconductivity persists in a wide class of materials without electron, or without hole pockets raises the question of how the Coulomb constraint is satisfied without loss of superconducting transition temperature.

In fact crystal symmetries do protect the *off-diagonal* Coulomb constraints. Within the subspace of dominant t_{2g}

orbitals, there are à priori six independent constraints. However, the off-diagonal components of F change sign under some of the non-symmorphic crystal symmetry operations and since an s-wave condensate is invariant under the crystal symmetries, the off-diagonal components of F must vanish, $F_{mm'} = 0$ ($m \neq m'$). For example, under a combined $\pi/2$ rotation about the z -axis and mirror-reflection in the xy plane, $(x, y, z) \rightarrow (y, -x, -z)$ and so $F_{zx,zy} \rightarrow -F_{zy,zx}$, which must then vanish for an s-wave condensate. Tetragonal crystalline symmetry also guarantees that $F_{zx,zx} = F_{zy,zy}$, are equal, so the Coulomb repulsion thus imposes two independent local constraints:

$$\begin{aligned} F_{zx,zx} &= F_{zy,zy} = 0, \\ F_{xy,xy} &= 0. \end{aligned} \quad (7)$$

In conventional phonon-paired superconductors the bare Coulomb repulsion is screened by virtual high energy pair fluctuations [22, 23]. This pair-screening process is logarithmically slow in energy, but the exponential separation of time-scales between the instantaneous Coulomb interaction and highly retarded electron-phonon interaction is sufficient to allow the electron-phonon interaction to win at low energies. This pair screening effect actually imposes a sign-change between the high- and low- frequency components of the Gor'kov function to satisfy the onsite equal-time constraint. In a purely-electronic pairing mechanism relevant to the FeSC, such a clean separation of time-scales is absent, so we can not appeal to retardation to impose the Coulomb constraint.

As such, the Coulomb problem is conceptually equal for FeSC with tetragonal or orthorhombic symmetry. We here concentrate on the case of fourfold rotational symmetry and mention that the orthorhombic symmetries also ensure vanishing off-diagonal components $F_{mm'}|_{m \neq m'}$ leading to three independent Coulomb conditions $F_{mm} = 0$.

B. Multiband Kohn-Luttinger physics: RG

A widely proposed mechanism for superconductivity from repulsive interactions relies on a generalization of the Kohn-Luttinger idea to multiband systems, often explored using renormalization group (RG) approaches [33–36]. These approaches have been used to argue that under a wide range of multi-band circumstances, the renormalization group flow develops an attractive pairing instability that overcomes the Coulomb constraint.

To illustrate these arguments and their connection to the Coulomb problem, we focus on two-band models. In this situation, the ladder resummation of logarithmic corrections to interband (intra-band) Cooper coupling constants G_{12} (G_{11}, G_{22}) is expressed in terms of two RG equations (see also App. B 3)

$$\frac{dg_{\pm}}{d \ln(D/T)} = -g_{\pm}^2, \quad (8)$$

Compound	FS	T_c		Ref.
monolayer FeSe	0h, 2e	65 K [‡]	on SrTiO ₃	[32]
Ba _{1-x} K _x Fe ₂ As ₂	2h, 2e	37 K	@ x = 0.4	[25, 26]
K _x Fe _{2-<i>y</i>} Se ₂	0h, 2e	30 K	@ (x,y) = (0.8, 0.3)	[31]
BaFe ₂ S ₃	quasi 1D	24 K	@ 10.6 GPa	[2, 3]
Ba(Fe _{1-x} Co _x) ₂ As ₂	2h [†] , 2e	22 K	@ x = 0.058	[27, 28]
Fe _{1+y} Se _x Te _{1-x}	3h, 2e	14.5 K	@ x = 0.45	[29, 30]
LaOFeP	2h, 2e	6K		[24]
KFe ₂ As ₂	3h*, 0e	4K		[6]

TABLE I. Summary of Fermisurface (FS) structure and T_c for a multitude of FeSC materials. The notation “ mh, ne ” means m hole pockets centered around the Γ point and n electron pockets. Footnotes: * There are additional 4 small hole pockets which are not centered around a high symmetry point. [†] 3D (i.e. non-cylindrical) character of the Fermi sheets, is important at the Γ point. [‡] T_c up to 109 K was reported in this material [4]. All references are based on ARPES, except [24], which is quantum oscillations, and [2, 3]. We are not aware of an experimental study of the electronic structure of BaFe₂S₃ (this material is insulating at ambient pressure). The ARPES data of these materials indicates a largest Fermi energy of 40 to 150 meV.

where we introduced the cutoff D , temperature T and

$$g_{\pm} = \frac{G_{11}\rho_1 + G_{22}\rho_2 \pm \sqrt{4G_{12}^2\rho_1\rho_2 + (G_{11}\rho_1 - G_{22}\rho_2)^2}}{2}. \quad (9)$$

Here $\rho_{1,2}$ denote density of states of the respective bands. While $g_+ > 0$ generically for repulsive interactions, g_- becomes negative for sufficiently strong interband interaction and its runaway flow signals the onset of s_{\pm} pairing. Importantly, $g_- < 0$ can be induced dynamically by fluctuations in the particle-hole channel (Kohn-Luttinger mechanism). Since the presence of a Cooper instability in Eq. (8) holds even for strong repulsion, these arguments suggest that the weak-coupling RG provides a resolution to the Coulomb problem.

However, a closer inspection reveals a difficulty with this line of reasoning. Each momentum space RG theory is tailor-made for a specific subset of FeSC compounds with the same Fermi surface topology, as such it does not provide a generic explanation for the robustness of the transition temperature against the appearance and disappearance of electron and hole pockets. Even within a family with a fixed Fermi surface topology the critical temperature suffers from unrealistically large variations as the relative carrier concentration in different pockets changes from compound to compound. We can illustrate this with the the two-band model. Suppose we concentrate on the limit of infinite repulsions where $G_{11} = G_{22} = G_{12} - g = U \rightarrow \infty$. While the robust existence of a Cooper instability in RG demonstrates an asymptotic orthogonalization against Coulomb repulsion, the microscopic on-site constraint, Eq. (7), is beyond its reach. In practice, this is reflected by a strong dependence of the UV value of the coupling constant

$$g_-(0) = g \frac{\rho_1 + \rho_2}{2} (1 - \delta^2) \quad (10)$$

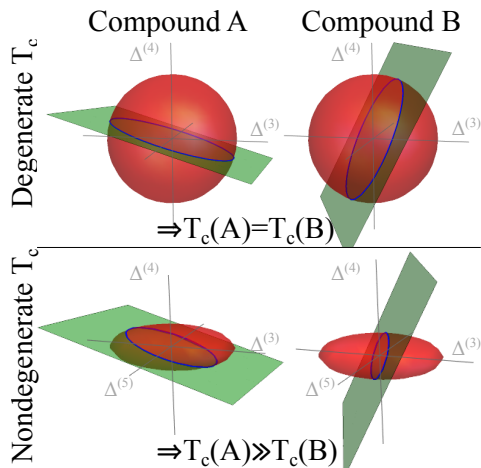


FIG. 1. Schematic illustrating orbital and k -space flexibility. Here, the large space of superconducting order parameters is represented as a three dimensional space. Each direction has an associated “bare” $T_c(\hat{\Delta})$ which is determined in the fictitious case without on-site repulsion and which is represented as the distance from the origin. It varies continuously and thus forms a surface, e.g. a sphere or an ellipsoid. The orientation with maximal T_c determines the pairing state. On-site Coulomb repulsion constraints the order parameter space to a submanifold, see Eq. (5). The latter is material dependent and represented by a plane. Upper panels: When the bare T_c is the same for all pairing directions, the orientation adapts to Coulomb repulsion without any cost in T_c (“orbital and k -space flexibility”). Lower panels (realistic situation): The bare T_c is direction dependent, orbital and k -space flexibility fails to explain comparable T_c for different materials.

on the relative density of states $\delta = (\rho_1 - \rho_2)/(\rho_1 + \rho_2)$, which leads to exponential suppression of $T_c = D \exp[-1/g_-(0)]$ when δ is of order unity. This strong suppression should be contrasted to the case of phononic BCS theory where, due to retardation, effects [22, 23], the effective Coulomb suppression μ^* is (i) weak and (ii) slowly dependent on UV physics. We conclude that RG only partially solves the Coulomb problem, and that search for a generic mechanism for Coulomb-protection is still unfulfilled.

C. Orbital and k -space Flexibility

A central element of the iron based superconductors, is the orbital degrees of freedom. In general, the gap function $\Delta_{m,m'}(\mathbf{k}) \equiv \langle m\mathbf{k} | \hat{\Delta} | m'\mathbf{k} \rangle$ is a momentum-dependent operator in the space of orbital quantum numbers. The simplest possibility is that pairing is orbitally trivial $\Delta_{m,m'}(\mathbf{k}) = \delta_{m,m'} \Delta(\mathbf{k})$. Another possibility, is orbitally selective pairing [37–39], in which the gap function is orbitally diagonal, but changes sign dependent on the orbital content $\Delta_{m,m'}(\mathbf{k}) = \delta_{m,m'} \Delta_m(\mathbf{k})$. The more general possibility, is *orbital entanglement* [40–42], in which the gap function is an off-diagonal matrix in the space of d -shell orbitals. For example,

$$\hat{\Delta} \propto |d_{xz}\rangle \langle d_{yz}| + |d_{yz}\rangle \langle d_{xz}|. \quad (11)$$

In this case, the condensate wave function can not be written as a product state in the space of orbitals, and is thus *orbitally entangled*. Sizeable interorbital, spin singlet pairing was predicted in material specific calculations on LiFeAs [43] and LaOFeAs [44]. Orbitally entangled spin triplet pairing has also been proposed for LaFeAsO_{1-x}F_x [45] and recently for LaNiGa₂ [46].

The robust appearance of superconductivity in a wide variety of Fermi surface morphologies, despite the absence of nodes in the gap to symmetry-protect against the Coulomb constraint, leads us to consider the possibility that the condensate takes advantage of the large number of s -wave pairing channels, adapting the orbital entanglement to minimize the Coulomb interaction. Such *orbital and k -space flexibility* (OKF) would hypothetically allow the condensate to “rotate” within a manifold of almost degenerate orbital pairing channels to satisfy the Coulomb constraint, approximately preserving the transition temperature, T_c (see Fig. 1). In this scenario, as the electronic structure changes from material to material, the pairing channel flexibly rearranges in response to the large space of Fermi-surface morphologies.

Motivated by these promising arguments, which are implicitly assumed in many theories of FeSC, we present a comprehensive study of orbital and k -space flexibility as a way to solve the Coulomb problem. Our principle conclusion, based on both phenomenological arguments and microscopic calculations, is that OKF requires an internal degeneracy amongst the pairing states. The apparent absence of such a degeneracy leads to a failure of orbital flexibility, forcing us to reconsider the singlet pairing assumption, as we discuss in the conclusions.

The paper is structured as follows: Section II is primarily phenomenological, and conceptually explains the Coulomb constraints and the idea of orbital and k -space flexibility. Sec. III provides a systematic classification of the superconducting matrix gap functions within the space of t_{2g} states and supporting, microscopic calculations. We summarize the derivation of the Landau theory and analyze a t - J model for a family of electronic structures. We conclude with a criticism and an outlook, Sec. IV, in which we discuss resolutions of the Coulomb conundrum beyond the spin-singlet s -wave channel.

II. LANDAU THEORY

In this section we cast the Coulomb problem in the iron based superconductors as a phenomenological Landau theory.

A. Coulomb repulsion in the free energy

Leaving microscopic details, a derivation and a thorough symmetry analysis to the subsequent Sec. III, we anticipate that a real order parameter, viz. a superconducting gap Δ_{Γ} , can be associated to each of the many pairing channels within the subspace of spin-singlet, extended s -wave states, see also Table II. Furthermore, in the present study of a three orbital

Γ	Name	$\varphi^\Gamma(\mathbf{k})\lambda_{i(\Gamma)}$	irrep
1.	conventional s-wave	λ_0	A_{1g}
2.	orbital-antiphase	λ_8	A_{1g}
3.	conventional s_\pm [47]	$c_x c_y \lambda_0$	A_{1g}
4.	orbitally-entangled [40–42]	$s_x s_y \lambda_1$	B_{2g}
5.	orbitally-selective	$(c_x - c_y)\lambda_3$	B_{1g}
6.	orbitally-antiphase s_\pm [37]	$c_x c_y \lambda_8$	A_{1g}

TABLE II. Summary of most relevant extended s-wave, spin singlet pairing channels as they appear in the expansion of the matrix gap function in irreducible representations of the point group $\Delta_{mm'}(\mathbf{k}) = \sum_{\Gamma=1}^{\mathcal{D}} \Delta_\Gamma \varphi^\Gamma(\mathbf{k})[\lambda_{i(\Gamma)}]_{mm'}$ (Gell-Mann matrices are denoted λ_i). We employed the notation $c_x = \cos(k_x)$, $s_x = \sin(k_x)$ etc. for the harmonics in the unfolded tetragonal Brillouin zone.

$$\mathcal{F} = -(\Delta_C, \Delta_P) \begin{pmatrix} \frac{\delta_{CC'}}{U_C} + \chi_{CC'} & \chi_{CP'} \\ \chi_{PC'} & -\frac{\delta_{PP'}}{g_P} + \chi_{PP'} \end{pmatrix} \begin{pmatrix} \Delta_{C'} \\ \Delta_{P'} \end{pmatrix} + \beta_{\Gamma_1\Gamma_2\Gamma_3\Gamma_4} \Delta_{\Gamma_1} \Delta_{\Gamma_2} \Delta_{\Gamma_3} \Delta_{\Gamma_4}. \quad (12)$$

Here we use the notation $\Gamma \rightarrow C \in \{1, 2\}$ to denote the two channels with repulsive Coulomb interaction U_C . On the other hand, we use $\Gamma \rightarrow P = 3, 4, \dots, \mathcal{D}$ to denote the attractive pairing channels with interaction g_P , for example s_\pm pairing and orbital entangled pairing. In Eq. (12) a summation over the repeated indices C, C', P and P' is implied and in the limit $U_C \rightarrow \infty$, we can omit the $1/U_C$ terms in the diagonal. The pair susceptibility $\chi_{\Gamma\Gamma'}$ is a matrix in the space of channels, illustrated diagrammatically in Fig. 2 along with the coefficients $\beta_{\Gamma_1\Gamma_2\Gamma_3\Gamma_4}$ of fourth order terms. Generically, the susceptibilities are finite, unless Γ and Γ' belong to different representations of the tetragonal group. However, sometimes there can be approximate cancellations brought on by cancellations between electron and hole pockets, as in the case of the s^\pm pairing scenario. The mean-field superconducting transition occurs at the first temperature where the first quadratic matrix develops a zero eigenvalue, corresponding to the condition

$$0 = \det \begin{pmatrix} \chi_{CC'} & \chi_{CP'} \\ \chi_{PC'} & -\frac{\delta_{PP'}}{g_P} + \chi_{PP'} \end{pmatrix} \\ = \det[\chi_{CC'}] \det \left[\chi_{PP'} - \chi_{PC} [\chi_{CC'}]^{-1} \chi_{C'P'} - \frac{\delta_{PP'}}{g_P} \right]. \quad (13)$$

The term including $[\chi_{CC'}]^{-1}$, which denotes the partial inverse in the subspace of repulsive channels, reduces the susceptibility $\chi_{PP'}$ of pairing channels and thereby suppresses T_c .

To illustrate these ideas, we analyze a two band model and compare to the discussion of Sec. IB. We restrict our attention to the Coulomb channel $C = 1$ and s^\pm pairing channel $P = 3$. In this case, the diagonal components of the pair susceptibility

model in the tetragonal phase, symmetries impose that exactly two such order parameters are penalized by the Coulomb energy. They represent intraorbital on-site pairing, see also Eq. (7). If we expand the Landau free energy in powers of the order parameters we obtain

are

$$\chi_{CC} \sim \chi_{PP} \sim \rho \ln \left(\frac{D}{T} \right) \quad (14)$$

where as the off-diagonal component is given approximately by

$$\chi_{CP} \sim \sum_{n=e,h} \int \frac{d^2k}{(2\pi)^2} c_x c_y \frac{\tanh \frac{\epsilon_{kn}}{2T}}{2\epsilon_{kn}} \sim \delta \rho \ln \left(\frac{D}{T} \right) \quad (15)$$

corresponding to a Fermi surface sum over the electron and hole pockets. Here, δ is a parameter that measures the average of $c_x c_y \equiv \cos(k_x) \cos(k_y)$ over the two compensating Fermi surface pockets, weighted by the density of states. This quantity vanishes when the density of states of the electron and hole pockets are fully compensated, but it grows to a number of order unity when either the electron or hole pockets are shrunk to zero. (Note that in a 2D band with strict quadratic dispersion, the density of states is independent of Fermi surface size, and in this extreme case δ only becomes sizeable at the Lifshitz transition where one Fermi surface vanishes.)

The condition for T_c is then given by

$$0 = \det \begin{pmatrix} \rho \ln \left(\frac{D}{T_c} \right) & \delta \rho \ln \left(\frac{D}{T_c} \right) \\ \delta \rho \ln \left(\frac{D}{T_c} \right) & \rho \ln \left(\frac{D}{T_c} \right) - \frac{1}{g} \end{pmatrix} \\ = \rho \ln \left(\frac{D}{T_c} \right) \left[\rho \ln \left(\frac{D}{T_c} \right) (1 - \delta^2) - \frac{1}{g} \right] \quad (16)$$

which gives

$$T_c = D \exp \left[-\frac{1}{g\rho(1 - \delta^2)} \right]. \quad (17)$$

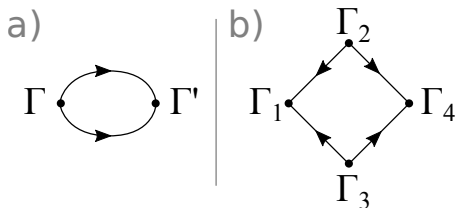


FIG. 2. Diagrammatic representation of the matrix pair susceptibility $\chi_{\Gamma\Gamma'}$ [panel a)] and the coefficients $\beta_{\Gamma_1\Gamma_2\Gamma_3\Gamma_4}$ [panel b)] which enter the Landau free energy, Eq. (12).

Thus once the cancellation between the electron and hole pockets is removed, the effect of the Coulomb interaction is to suppress the effective coupling constant $g\rho \rightarrow g\rho(1 - \delta^2)$, producing an exponential depression in the transition temperature. Yet experimentally, the elimination of the hole pockets in iron selenides produces no significant reduction in T_c .

Note that this same result (17) can also be obtained using RG method (8) with starting value $g_-(0)$ given in Eq. (10). However, the physical discrepancy between the implications of Eq. (17) and experimental reality is independent of the theoretical approach. This prompts us to enquire whether the re-introduction of additional orbitals and pairing channels will provide an additional flexibility to avoid the strong dependence of T_c on Fermi surface structure seen in this simple example.

We conclude this section with a comment on the incipient band scenario: It has been demonstrated, that bands which do not cross the Fermi level but reside within a distance D in energy space facilitate superconductivity [48, 49]. Formally, this is because also incipient bands may contribute large logarithms to $\chi_{P,P'}$. At the same time, the incipient band scenario can not provide a generic reason why the term including $[\chi_{CC'}]^{-1}$ in Eq. (13) should be generically negligible in FeSC and can not solve the Coulomb problem generically.

B. Landau formulation of orbital and k-space flexibility

The Landau energy has the following salient features: First, the quadratic part of the attractive channels is determined by a matrix

$$[\underline{\epsilon}(T)]_{PP'} = \frac{\delta_{PP'}}{g_P} - \chi_{PP'}, \quad (18)$$

which is positive definite for $T > T_c$ and has lowest eigenvalue proportional to $(T - T_c)/T_c^2$, its associated eigenvector \hat{e} determining the direction of the instability in channel space. Second, in order to avoid the energetically cost of Coulomb repulsion, the on-site pair density, i.e. Gor'kov function, must vanish. Expanding $F_{m,m'}(\mathbf{k})$ in s -wave channels, Eq. (5) becomes $F_C = \chi_{CC'}\Delta_{C'} + \chi_{CP}\Delta_P = 0$ with $C = 1, 2$. The solution $\Delta_C = -[\chi_{CC'}]^{-1}\chi_{C'P}\Delta_P$ implies a reduction of the $\chi_{PP'}$ susceptibility, see also Eq. (13), unless the vector $\vec{\Delta}_P = (\Delta_3, \Delta_4, \dots)$ of superconducting order parameters is orthogonal to the vectors formed from the inter-channel pair

susceptibilities $\vec{\chi}_C \equiv \chi_{CP} = (\chi_{C3}, \chi_{C4}, \dots)$ ($C=1,2$). Consequently, T_c is reduced unless

$$0 = \vec{\chi}_C \cdot \vec{\Delta}_P. \quad (19)$$

We shall make two assumptions about the vectors χ_{1P}, χ_{2P} and the matrix $\underline{\epsilon}(T)$. First, both vectors and $\underline{\epsilon}(T)$ are highly susceptible to changes in the electronic structure, in particular the Fermi surface geometry. Second, $\chi_{1P} = 0 = \chi_{2P}$ if the order parameter in pairing channel P transforms according to a different representation than s -wave even-frequency (e.g. if P was a d -wave channel). In this case Eq. (19) is automatically fulfilled. In contrast, we here concentrate on the case in which $\chi_{CP} \neq 0$ in general, scrutinize another explanation, i.e. orbital and k -space flexibility, and therefore ask the following questions: does the large dimension \mathcal{D} of the order parameter space provide a credible mechanism for the FeSC to adapt to the strong on-site Coulomb repulsion? Moreover, is this mechanism applicable within the subspace of extended s -wave states?

The appeal of the OKF concept, lies in the observation that while there may be several attractive pairing channels, there are only two Coulomb constraints Eq. (19). Although this lowers the dimension of the manifold of attractive states from \mathcal{D} to $\mathcal{D} - 2$, so long as a Cooper instability survives in one of the many pairing channels which remain, it would seem plausible that the pairing state can smoothly adapt to the Coulomb repulsion. The hope is that this mechanism prevents or at least weakens the reduction of T_c due to Coulomb repulsion.

In order to further develop this idea we first consider the case in which the lowest eigenvalue of the matrix $\underline{\epsilon}(T)$ is almost degenerate, i.e. just below T_c there are a number of nearby superconducting instabilities corresponding to a sequence of small eigenvalues proportional to $(T - T_c^{(2)}), (T - T_c^{(3)}), \dots$ with $T_c - T_c^{(2,3,\dots)} \ll T_c$. If the degeneracy is sufficiently large, changes to T_c will remain small even though the vector space of allowed states perpendicular to χ_{1P}, χ_{2P} would undergo a large-scale rotation when the electronic structure changes from compound to compound.

The above discussion demonstrates the potential of the OKF mechanism to overcome the Coulomb repulsion by exploiting the large manifold of degenerate pairing states (see Fig. 1, upper panels). In particular, the orbital degrees of freedom increase the flexibility by introducing orbital selective and orbital entangled Cooper channels which allow to orthogonalize against Coulomb interaction in orbital space.

III. SYMMETRIES AND MICROSCOPICS

In the previous section, the concept of OKF was qualitatively elaborated on the level of a phenomenological Landau theory. In this section, we provide quantitative aspects regarding the large multitude of pairing states, i.e. the fundamental ingredient for OKF, in iron-based superconductors. We will focus on the three t_{2g} -orbitals in a purely 2D model, though our discussion can be simply extended to a more general setup. We first provide a symmetry classification of states and then present a microscopic calculation.

A. Superconducting states and crystal symmetries

The matrix gap function $\Delta(\mathbf{k})$ can naturally be expanded in irreducible representations of the point group

$$\Delta_{mm'}(\mathbf{k}) = \sum_{\Gamma=1}^D \Delta_{\Gamma} \varphi^{\Gamma}(\mathbf{k}) [\lambda_{i(\Gamma)}]_{mm'}. \quad (20)$$

Here, λ_i are the Gell-Mann matrices (see Appendix A 4). A comprehensive classification [50] of all states based on the crystal symmetries is summarized in Table II, with more details given in appendix A and an illustration presented in Fig. 3. The coefficients Δ_{Γ} are real, provided time-reversal symmetry is unbroken. For spin singlet pairs, the exclusion principle forces the spatial wavefunction to be even, so that the *combined* form factors $\varphi^{\Gamma}(\mathbf{k})\lambda_{i(\Gamma)}$ are even under simultaneous spatial inversion and matrix transposition. Point group operations, such as a π rotation in the iron plane $\mathbf{k} \rightarrow R_{\pi}\mathbf{k} = (-k_x, -k_y, k_z)$, are represented by unitary matrices in orbital space, e.g. $U_{R_{\pi}} = \text{diag}(-1, -1, 1)$. We adopt a convention in which the orbitals are placed in the order $m = (1, 2, 3) \equiv (d_{xz}, d_{yz}, d_{xy})$. Assuming the order parameter has overall s-wave symmetry, it must remain invariant under the crystal transformations,

$$\Delta(\mathbf{k}) = U_{R_{\pi}}^{\dagger} \Delta(R_{\pi}\mathbf{k}) U_{R_{\pi}}. \quad (21)$$

Still, non-trivial (e.g. B_{1g}) form factors $\varphi^{\Gamma}(\mathbf{k})$ are possible, as long as the transformation behavior of associated Gell-Mann matrices $\lambda_{i(\Gamma)}$ compensates the transformation behavior of $\varphi^{\Gamma}(\mathbf{k})$.

In Table II we stretch our notation beyond standard group theoretical convention and use different Γ indices for form factors $\varphi^{\Gamma}(\mathbf{k})$ of the same irreducible representation, but with different Fourier harmonics. This allows to distinguish physically distinct states with the same transformation properties, e.g. conventional s-wave from the s_{\pm} or orbital entangled states. This description can be extended in various ways, e.g. to include higher angular momentum or odd-frequency pairing [51].

B. Derivation of Landau theory

A BCS description of the interactions in these various channels then takes the form

$$H_I = \sum_{C=1,2} U_C \Psi_C^{\dagger} \Psi_C - \sum_{P=3,\dots} g_P \Psi_P^{\dagger} \Psi_P, \quad (22)$$

where we use $C \equiv \Gamma_C$ to denote the repulsive Coulomb channels and $P \equiv \Gamma_P$ to denote the attractive pairing channels. The pair creation operators take the form

$$\Psi_{\Gamma}^{\dagger} = \sum_{\mathbf{k}, m, m'} \varphi^{\Gamma}(\mathbf{k}) \lambda_{m, m'}^{\Gamma} \left(c_{\mathbf{k}m\uparrow}^{\dagger} c_{-\mathbf{k}m'\downarrow}^{\dagger} - (\uparrow\leftrightarrow\downarrow) \right), \quad (23)$$

where the sum is over an energy shell $|\epsilon_{\mathbf{k}}| \leq D$ around the Fermi surface.

We typically carry out a Hubbard-Stratonovich transformation of the repulsive and attractive interactions, so that the interactions can be written in a mean-field form

$$H_I = \sum_{\Gamma} (\Delta_{\Gamma} \Psi_{\Gamma} + \text{H.c.}) - \sum_{C=1,2} \frac{|\Delta_C|^2}{U_C} + \sum_{P=3,\dots} \frac{|\Delta_P|^2}{g_P}. \quad (24)$$

This kind of transformation is carried out with the understanding that inside the path integral, the Coulomb gap variables are integrated along the imaginary axis $\Delta_C \in [-i\infty, i\infty]$, but that in a mean-field theory, we can distort the contour and seek a saddle point solution where the Δ_C lie on the real axis. The combined set of order parameters $\Delta_{\Gamma} = (\Delta_C, \Delta_P)$ then form a D dimensional real vector.

We are particularly interested in the limit where the $U_C \rightarrow \infty$ are large enough to neglect the second term. In this case, the saddle point values of the Δ_C ($C=1,2$) play the role of Lagrange multipliers that impose the Coulomb constraints $\langle \Psi_C \rangle = 0$ ($C=1,2$), equivalent to conditions (7).

The derivation of the Landau free energy follows from the integration of fermionic degrees of freedom. The generic form for the pair susceptibility matrix entering Eq. (12) is given by

$$\chi_{\Gamma\Gamma'} = \sum_{n, n'} \int \frac{d^2k}{(2\pi)^2} \varphi_{n, n'}^{\Gamma}(\mathbf{k}) \varphi_{n', n}^{\Gamma'}(\mathbf{k}) \frac{1 - f(\epsilon_{kn}) - f(\epsilon_{kn'})}{\epsilon_{kn} + \epsilon_{kn'}}. \quad (25)$$

where n is the band-index and the

$$\varphi_{n, n'}^{\Gamma}(\mathbf{k}) = \varphi^{\Gamma}(\mathbf{k}) \sum_{m, m'} \langle \mathbf{k}n | m \rangle \lambda_{m, m'}^{\Gamma} \langle m' | \mathbf{k}n \rangle \quad (26)$$

are the form-factors of the pairing matrices in the band-basis. The interband ($n \neq n'$) parts of these matrices are weakly temperature dependent. However, the intra-band parts ($n = n'$) contain a Cooper-instability divergence

$$\chi_{\Gamma\Gamma'}(T) = \rho_{\Gamma\Gamma'} \ln \frac{D}{T} \quad (27)$$

where

$$\rho_{\Gamma\Gamma'} = \sum_n \rho_n \left\langle \varphi_{nn}^{\Gamma}(\mathbf{k}) \varphi_{nn}^{\Gamma'}(\mathbf{k}) \right\rangle_{FS} \quad (28)$$

where ρ_n is the density of states for the n -th Fermi surface and $\langle \dots \rangle_{FS}$ represents the corresponding Fermi surface average.

C. Generalized t-J model

In this section we investigate our findings by means of a microscopic t-J model (without a constraint on the occupancy) treated to the mean field level. In addition to the on-site interaction (3) we consider nearest neighbor antiferromagnetic coupling J_1 and next nearest neighbor antiferromagnetic coupling J_2 ,

$$H_{J_1} = \sum_{mm'} \sum_{\mathbf{k}} J_1^{mm'} (c_x + c_y) : \mathbf{S}_{m, \mathbf{k}} \cdot \mathbf{S}_{m', -\mathbf{k}} :, \quad (29a)$$

$$H_{J_2} = \sum_{mm'} \sum_{\mathbf{k}} J_2^{mm'} c_x c_y : \mathbf{S}_{m, \mathbf{k}} \cdot \mathbf{S}_{m', -\mathbf{k}} :. \quad (29b)$$

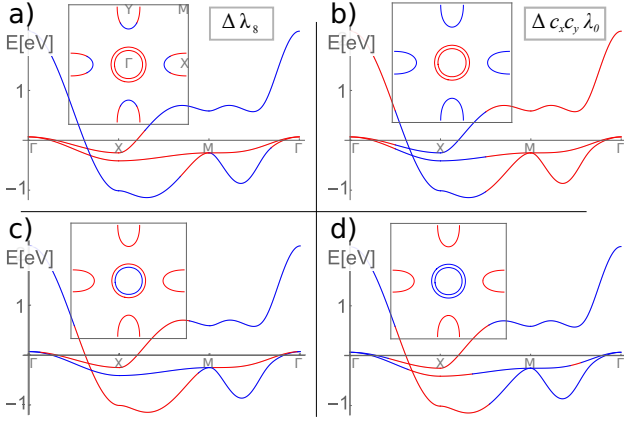


FIG. 3. Graphical representation of several superconducting states based on the tight binding model proposed in Ref. [52]. The dispersion relation along $\Gamma - X - M - \Gamma$ is colored red (blue) for positive (negative) sign of the gap function. Each panel also contains an inset where the Fermi surfaces are plotted with the same color coding. Panel a): Orbital antiphase, $\Delta(\mathbf{k}) = \Delta\lambda_8$ (in the present tight binding model, this state has nodes). Panel b): Conventional s_{\pm} , $\Delta(\mathbf{k}) = \Delta c_x c_y \lambda_0$. Panel c): A mixed state $\Delta(\mathbf{k}) = \Delta(-0.01c_x c_y \lambda_0 - 0.99s_x s_y \lambda_1 + 0.11(c_x - c_y)\lambda_3)$ with strong orbital entanglement. Panel d): A mixed state $\Delta(\mathbf{k}) = \Delta(-0.97c_x c_y \lambda_0 - 0.03s_x s_y \lambda_1 + 0.24(c_x - c_y)\lambda_3)$ which is mainly s_{\pm} . Panel c) [d)] occurs at $x = -0.9$ [$x = 0.7$] in the microscopic calculation of Fig. 4. Note that orbital entanglement naturally explains the sign change within the two inner Fermi surfaces of hole doped FeSC as proposed in [53].

We note that inter-orbital magnetic interactions are not uncommon, e.g. perfectly Hund's aligned antiferromagnetic interaction can be expected to be of the form $J\mathbf{S}_{\text{total},1} \cdot \mathbf{S}_{\text{total},2} = J(\sum_m \mathbf{S}_{m,1}) \cdot (\sum_{m'} \mathbf{S}_{m',2})$ projected onto the strong Hund's subspace.

In Appendix B 1, we project the interactions on the space of spin singlet pairing. The magnetic interactions generate Cooper channel attraction in extended s-wave and, for concreteness, we assume that Cooper instabilities occur only in channels $\Gamma = 3 - 5$, so that the effective Landau free energy, (12), is determined by only three attractive interactions

$$g_3 = [2J_2^{xz,xz} + J_2^{xy,xy}]/4, \quad (30a)$$

$$g_4 = [3J_2^{xz,yz}]/4, \quad (30b)$$

$$g_5 = [3J_1^{xz,xz}]/8, \quad (30c)$$

and repulsions $U_1 = U_2 = [U + 3J_{H,1}/2]/2 \equiv \bar{U}/2$. We used $J_2^{xz,xz} = J_2^{yz,yz}$ due to crystal symmetries.

In Fig. 4 we numerically evaluate T_c for the given system and introduce a parameter $x \in (-1, 1)$ to interpolate between the hole dominated case at $x = -1$ to an electron dominated case at $x = 1$. We assume $[2J_2^{xz,xz} + J_2^{xy,xy}]/3 = J_2^{xz,yz} = 2J_1^{xz,xz} \equiv J/2$ and Fermi surfaces with the orbital content and geometry analogous to those [52] represented in Fig. 3. We compare our results to the fictitious case of a system in which orbital and k-space flexibility are not allowed. Clearly, the system takes advantage of its flexibility, the instability changes direction from $(\Delta_3, \Delta_4, \Delta_5) \propto (0, -0.99, 0.11)$ at

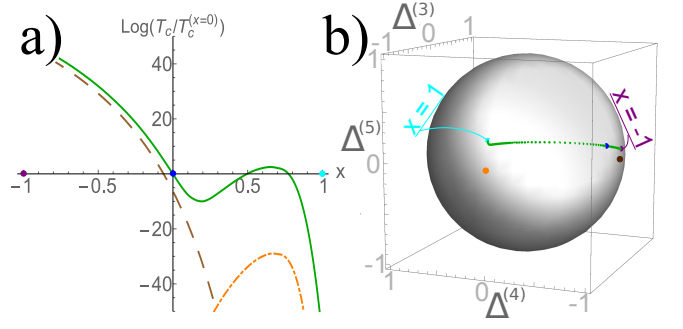


FIG. 4. Microscopic investigation of orbital flexibility based on Eqs. (12), (30) of the main text. The parameter x is introduced in the density of states $\rho_e = (1+x)/(20J)$ ($\rho_h = (1-x)/(10J)$) of electron pockets (hole pockets) in order to smoothly interpolate between systems with different types of carriers. Panel a): Evolution of T_c as a function of x , the solid/dashed/dotted curves represent T_c for the flexible/the Δ_4 /the Δ_3 state, all of which are normalized to the T_c of the flexible state at $x = 0$. Panel b): Evolution of the direction of the flexible state in the space of $\Delta_{3,4,5}$. For this plot we chose a moderate $\bar{U}/J = 3$. For $\bar{U}/J = 10$ the graphs of both panels are qualitatively similar, however the local maximum near $x \approx 0.7$ drops down to $\ln(T_c/T_c^{(x=0)}) \approx -20$.

$x = -1$ to $(\Delta_3, \Delta_4, \Delta_5) \propto (-0.97, -0.03, 0.24)$ at $x = 0.7$, the position of optimal electron doping, see Fig. 3 c) and d) for an illustration of these orbital entangled and orbital selective states. Panel a) of Fig 4 demonstrates how the system adapts from following $T_c^{(4)}$ in channel Δ_4 to the $T_c^{(3)}$ of Δ_3 as soon as the orange dotted curve overtakes the brown dashed curve. However, Fig. 4 also demonstrates, that the maximum $T_c^{(3)}$ and the maximum $T_c^{(4)}$ are generically well separated, even for the present choice of equal attractive interaction in the two channels. This results in $\ln[T_c^{(x=-1)}/T_c^{(x=0.7)}] \sim 40$ for the present choice $\bar{U}/J = 3$, which is gigantic and increases further as \bar{U}/J increases. These observations are the basis for the criticism of OKF presented in the next section.

IV. CRITIQUE AND OUTLOOK

A key result of our investigation of the effects of onsite Coulomb interactions in the iron-based superconductors, is that observation that Coulomb repulsion enforces two constraints on the condensate, forcing two on-site, equal-time pairing amplitudes to vanish, see Eq. (19). In most unconventional superconductors, these Coulomb constraints are symmetry-protected through the development of higher angular momentum condensates, for which the Coulomb constraint is automatically satisfied. Current extended s-wave theories of the iron-based superconductors have difficulty explaining how the Coulomb constraint is satisfied for a wide variety of Fermi surface morphologies, without marked suppression of T_c . A key question is whether there is some kind of hidden or accidental symmetry in FeSC?

We attempted to provide a way out of this conundrum, examining a hypothesis that pairing within a large class of or-

bitally entangled singlet states allows the condensate the orbital and k-space flexibility (OKF) to “rotate” into new configurations that satisfy the Coulomb constraint in new Fermi surface morphologies. We encountered a number of unresolved issues with the OKF approach:

1. OKF requires that the lowest eigenvalues of the matrix $\underline{\epsilon}(T)$ must be almost degenerate, see Sec. II. [54]
2. From a microscopic weak-coupling viewpoint, different Fermi surface geometries lead to different pair susceptibility matrices. Therefore, even if the lowest eigenvalue of $\underline{\epsilon}(T)$ was largely degenerate for a given compound, it is unlikely to be so in another. This would lead to dramatic variations in T_c from compound to compound, see Fig. 1, lower panels.
3. Concerning k-space flexibility, one would like to concentrate on states involving only the first few harmonics, since higher harmonics require long-distance interactions. This substantially reduces the dimension \mathcal{D} of the order parameter space. Finally, it is worth mentioning that a linear increase in the lowest eigenvalue of $\underline{\epsilon}$ implies an exponential decrease of T_c within microscopic weak-coupling theories, due to the logarithmic Cooper instability.

These arguments suggest that orbital and k-space flexibility is unable to explain the robustness of T_c against Coulomb repulsion in the zoo of FeSC. Our microscopic calculations leading to Fig. 4 corroborate this conclusion. The OKF mechanism requires a well-protected degeneracy of transition temperatures, which in turn would require an underlying symmetry which is simply absent for an orbitally entangled s-wave condensate.

In the present analysis, only Cooper channel instabilities were considered in a simple mean field treatment. More generally particle-hole channels should also be taken into account. As we mentioned in the introduction and in Sec. IB, while the mutual renormalizations of particle-hole and particle-particle channels can provide a mechanism to reverse the sign of Coulomb interaction near the scale of the superconducting instability, the results are still highly sensitive to the Fermi surface morphology and the pattern of bare repulsive interaction values [36]. In short, the existing weak-coupling RG scenarios are unable to account for the robustness against changes of Fermi surface morphologies as T_c strongly depends on ultraviolet scales.

What alternative mechanisms for robustly avoiding the Coulomb problem might be at work across the full range of iron-based superconductors? One possibility we are forced to reconsider, is that pairing in the FeSC is not primarily driven by extended s-wave, spin singlet pairing, but that it involves a symmetry-protected orthogonalization against Coulomb interaction. One way forward is to explore higher angular momentum states in the spin singlet channel. Many proposals in the literature have examined d-wave [38, 39, 55, 56] pairing.

The common observation of full excitation gaps remains an open issue for higher angular momentum states (see Ref. [38] for a thorough discussion of the disappearance of nodes). A second way forward is to consider spin triplet pairing. Apart

from early p-wave proposals [57], the orbital degrees of freedom allow for the formation of condensates which are anti-symmetric in orbital space. Such “orbital singlet”, spin triplet pairing [58, 59] can occur in an s-wave channel. The classic objection to spin triplet pairing is the observation of a Knight shift. However, spin orbit coupling can lead to spin singlet admixture. Indeed, the Knight shift in the spin triplet superfluid ^3He is actually sizeable, in part because of spin-orbit coupling [60]. Finally, odd-frequency pairing might find another route to orthogonalization against the Coulomb constraints. While such a state does not develop a spectral gap on its own, it may couple to pairing channels in which the gap matrix and the kinetic part Hamiltonian do not commute and thus indirectly induce a gap.

V. ACKNOWLEDGEMENTS

We acknowledge valuable discussions with T. Ayrál, P.-Y. Chang and Y. Komijani. This material is based upon work supported by the U.S. Department of Energy, Office of Science, Office of Basic Energy Sciences, under Award DE-FG02-99ER45790 (Elio Koenig and Piers Coleman).

Appendix A: Classification of the order parameter matrix within the three band model

This Appendix reviews the crystal symmetries of iron based superconductors and deduces their implications for the kinetic energy and pairing components of the Hamiltonian within the space of t_{2g} orbitals. This provides us with a comprehensive classification of superconducting states within the three-orbital model. This work extends earlier work [50] to the case of band-off-diagonal gap functions, which in turn implies [61] odd frequency pairing.

Consider the following Gor’kov Green’s function

$$\mathcal{G}_k(\tau) = -\langle T\Psi_k(\tau)\Psi_k^\dagger(0) \rangle. \quad (\text{A1})$$

Here the Nambu spinors Ψ_k are composed from fermionic creation and annihilation operators $c_{k,\alpha,m}^\dagger, c_{k,\alpha,m}$ in the standard way $\Psi_k = (c_{k,\uparrow}^\dagger, c_{-k,\downarrow}^\dagger)^T$ and $\Psi_k^\dagger = (c_{k,\uparrow}^\dagger, c_{-k,\downarrow}^\dagger)$. The transposition symbol indicates that creation (annihilation) operators are grouped into row (column) three-vectors and we choose to order orbitals $m = d_{xz}, d_{yz}, d_{xy}$ from left to right (top to bottom). The Gor’kov Green’s function is a matrix in Nambu space which, in frequency representation, can be displayed as

$$\mathcal{G}_{\omega_n, \mathbf{k}} = \begin{pmatrix} G_{\omega_n, \mathbf{k}}^{(e)} & F_{\omega_n, \mathbf{k}} \\ F_{-\omega_n, \mathbf{k}}^\dagger & G_{\omega_n, \mathbf{k}}^{(h)} \end{pmatrix} \quad (\text{A2a})$$

$$= \begin{pmatrix} i\omega_n - H_{\mathbf{k}} - \Sigma_{\omega_n, \mathbf{k}} & -\Delta_{\omega_n, \mathbf{k}} \\ -\Delta_{-\omega_n, \mathbf{k}}^\dagger & i\omega_n + H_{-\mathbf{k}}^T + \Sigma_{-\omega_n, -\mathbf{k}}^T \end{pmatrix}^{-1}. \quad (\text{A2b})$$

All entries of these matrices are themselves three by three matrices in orbital space. We used $\mathcal{G}_{\omega_n, \mathbf{k}} = \mathcal{G}_{-\omega_n, \mathbf{k}}^\dagger$, cf. the

$\alpha_1 \leftrightarrow \alpha_2$	$\omega_n \leftrightarrow -\omega_n$	$\mathbf{k} \leftrightarrow -\mathbf{k}$	$m_1 \leftrightarrow m_2$	Details
-	+	+	+	Table IV
-	+	-	-	Table V
-	-	+	-	Table VI
-	-	-	+	Table VII

TABLE III. Summary of superconducting singlet states for the three-orbital model of the iron-based superconductors. The first column refers to the parity under exchange of the spins of the constituent electrons of the Cooper pairs. The second and third column refer to the parity under temporal or spatial inversion of the order parameter function. The fourth column describes the parity under transposition in the space of t_{2g} orbitals. By assumption, the order parameter field is in a singlet state and thus odd under exchange of spin. For each row, Pauli's principle imposes a negative sign upon multiplication of columns one through four. The last column refers to tables IV - VII containing more details on each of the four category of states.

definition (A1), so that electron and hole Green's functions satisfy $G_{\omega_n, \mathbf{k}}^{(e,h)} = [G_{-\omega_n, -\mathbf{k}}^{(e,h)}]^\dagger$. In the second line, we relate the Gor'kov Green's function to the kinetic part of the Hamiltonian $H_{\mathbf{k}}$, a self-energy $\Sigma_{\omega_n, \mathbf{k}} = \Sigma_{-\omega_n, -\mathbf{k}}^\dagger$ and a gap function $\Delta_{\omega_n, \mathbf{k}}$. In full generality, the order parameter F and gap Δ matrices may be frequency dependent, for a comment on the subtlety of the reversed frequency in the lower left matrix element see Sec. A3.

1. Symmetry operations

As we mentioned in the main text, we are interested in singlet pairing. The Pauli principle imposes (see also Table III)

$$F_{\omega_n, \mathbf{k}} = F_{-\omega_n, -\mathbf{k}}^T, \quad \Delta_{\omega_n, \mathbf{k}} = \Delta_{-\omega_n, -\mathbf{k}}^T. \quad (\text{A3})$$

Furthermore, time reversal symmetry implies $\mathcal{G}_{\omega_n, \mathbf{k}} = \mathcal{G}_{\omega_n, -\mathbf{k}}^T$ so that $G_{\omega_n, \mathbf{k}}^{(e,h)} = (G_{\omega_n, -\mathbf{k}}^{(e,h)})^T$, $H_{\mathbf{k}} = H_{-\mathbf{k}}^T$, and $\Sigma_{\omega_n, \mathbf{k}} = \Sigma_{\omega_n, -\mathbf{k}}^T$ as well as hermiticity of the anomalous Green's function and the gap matrix

$$F_{\omega_n, \mathbf{k}} = F_{\omega_n, \mathbf{k}}^\dagger, \quad \Delta_{\omega_n, \mathbf{k}} = \Delta_{\omega_n, \mathbf{k}}^\dagger. \quad (\text{A4})$$

Since the chalcogen/pnictogen atoms are ordered above and below the iron plane in an alternating manner, the system has a two-atom unit cell which in iron-only models shows up as staggered hopping elements. We choose the origin on an iron site for the lattice model represented by Fig 5.

There are two mirror symmetries

$$\begin{aligned} \mathcal{G}_{\omega_n, \mathbf{k}} &= \begin{pmatrix} 1 & 0 & 0 \\ 0 & -1 & 0 \\ 0 & 0 & -1 \end{pmatrix} \mathcal{G}_{\omega_n, \hat{P}_x \hat{P}_z \mathbf{k}} \begin{pmatrix} 1 & 0 & 0 \\ 0 & -1 & 0 \\ 0 & 0 & -1 \end{pmatrix} \\ &= \begin{pmatrix} -1 & 0 & 0 \\ 0 & 1 & 0 \\ 0 & 0 & -1 \end{pmatrix} \mathcal{G}_{\omega_n, \hat{P}_y \hat{P}_z \mathbf{k}} \begin{pmatrix} -1 & 0 & 0 \\ 0 & 1 & 0 \\ 0 & 0 & -1 \end{pmatrix} \end{aligned} \quad (\text{A5a})$$

and a C_4 rotation symmetry

$$\mathcal{G}_{\omega_n, \mathbf{k}} = \begin{pmatrix} 0 & 1 & 0 \\ -1 & 0 & 0 \\ 0 & 0 & -1 \end{pmatrix} \mathcal{G}_{\omega_n, \hat{R}_{\pi/2} \hat{P}_z \mathbf{k}} \begin{pmatrix} 0 & -1 & 0 \\ 1 & 0 & 0 \\ 0 & 0 & -1 \end{pmatrix}. \quad (\text{A6})$$

Here we have introduced a set of three inversion operators ($\hat{P}_x, \hat{P}_y, \hat{P}_z$) which respectively reverse the x, y and z components of momentum, and a rotation $\hat{R}_{\pi/2} : (k_x, k_y, k_z) \rightarrow (k_y, -k_x, k_z)$.

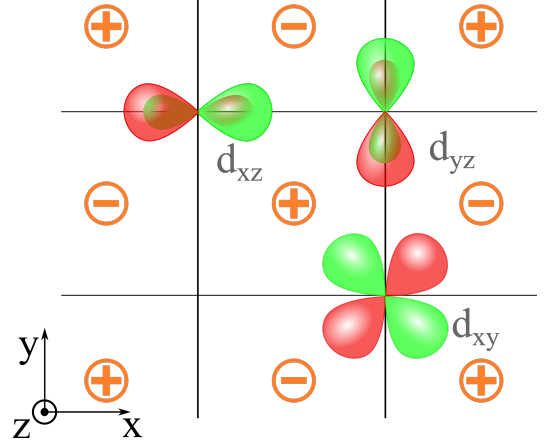


FIG. 5. Representation of the three t_{2g} orbitals in an iron plane. The sites of the lattice correspond to iron positions. Chalcogen/pnictogen atoms reside in alternating positions above/below a plaquette (indicated by a circle with a plus/minus sign). The sign of the lobes of the orbitals is represented by two different colors: light green and darker red.

2. Even frequency pairing

Often, superconducting order parameters are assumed to be an even function of frequency (in most cases a constant). We denote such states by a “+” in the subscript of the order parameter $F_{\omega_n, \mathbf{k}, +}$ and gap $\Delta_{\omega_n, \mathbf{k}, +}$. According to Eqs. (A3), (A4) these matrix functions transform in the same manner as the kinetic part of the Hamiltonian under crystal and time reversal symmetries. It is convenient to expand the order parameter matrix by means of Gell-Mann matrices (see Appendix A4)

$$F_{\omega_n, \mathbf{k}, +} = \sum_{i=0}^8 F_{\omega_n, \mathbf{k}, +}^{(i)} \lambda_i. \quad (\text{A7})$$

The gap function $\Delta_{\omega_n, \mathbf{k}, +}$ and the diagonal parts of the (inverse) Green's function, and the Hamiltonian are expanded analogously. The transformation behavior of each function $F_{\omega_n, \mathbf{k}, +}^{(i)}, \Delta_{\omega_n, \mathbf{k}, +}^{(i)}$, etc. may be found in Table IV and Table V, corresponding to symmetric and antisymmetric Gell-Mann matrices, respectively. We note that, in a purely 2D model where $k_z = 0$, the coefficients of $\lambda_{2,4,6}$ vanish by symmetry.

i	\hat{P}_x	\hat{P}_y	\hat{P}_z	$\hat{R}_{\pi/2}$	examples
0	+	+	+	+	$1, c_z, c_x c_y$
1	-	-	+	-	$s_x s_y$
3	+	+	+	-	$(c_x - c_y)$
$\begin{pmatrix} 4 \\ 6 \end{pmatrix}$	$\begin{pmatrix} + & 0 \\ 0 & - \end{pmatrix}$	$\begin{pmatrix} - & 0 \\ 0 & + \end{pmatrix}$	$\begin{pmatrix} - & 0 \\ 0 & - \end{pmatrix}$	$\begin{pmatrix} 0 & - \\ + & 0 \end{pmatrix}$	$\begin{pmatrix} s_y s_z \\ s_x s_z \end{pmatrix}$
8	+	+	+	+	$1, c_z, c_x c_y$

TABLE IV. Transformation behavior of coefficients $F_{\omega_n, \mathbf{k}, +}^{(i)}, \Delta_{\omega_n, \mathbf{k}, +}^{(i)}, H_{\mathbf{k}}^{(i)}$, see Eq. (A7), which are even under all of $\omega_n \rightarrow -\omega_n, \mathbf{k} \rightarrow -\mathbf{k}$ and transposition in orbital space. The signs indicate the parity under reflections and under $\pi/2$ rotations in the iron plane. The functions ($F_{\omega_n, \mathbf{k}, +}^{(4)}, F_{\omega_n, \mathbf{k}, +}^{(6)}$) (and analogously for $\Delta_{\omega_n, \mathbf{k}}$ and $H_{\mathbf{k}}$) transform under a two dimensional representation. These two functions get interchanged under a $\pi/2$ rotation. The last column displays the leading harmonics.

i	\hat{P}_x	\hat{P}_y	\hat{P}_z	$\hat{R}_{\pi/2}$	examples
2	+	+	-	-	$(c_x - c_y) s_z$
$\begin{pmatrix} 5 \\ 7 \end{pmatrix}$	$\begin{pmatrix} - & 0 \\ 0 & + \end{pmatrix}$	$\begin{pmatrix} + & 0 \\ 0 & - \end{pmatrix}$	$\begin{pmatrix} + & 0 \\ 0 & + \end{pmatrix}$	$\begin{pmatrix} 0 & + \\ - & 0 \end{pmatrix}$	$\begin{pmatrix} s_x \\ s_y \end{pmatrix}$

TABLE V. Transformation behavior of coefficients $F_{\omega_n, \mathbf{k}, +}^{(i)}, \Delta_{\omega_n, \mathbf{k}, +}^{(i)}, H_{\mathbf{k}}^{(i)}$, see Eq. (A7), which are even under $\omega_n \rightarrow -\omega_n$ but odd under $\mathbf{k} \rightarrow -\mathbf{k}$ and transposition in orbital space. The notation is the same as in Table IV.

3. Odd frequency pairing

Odd frequency components [51] of the order parameter and gap matrix, which we denote as $F_{\omega_n, \mathbf{k}, -}, \Delta_{\omega_n, \mathbf{k}, -}$ are generally considered to be more exotic than even-frequency states. However, in multiband materials, odd-frequency components $F_{\omega_n, \mathbf{k}, -}$ are also induced by an even $\Delta_{\omega_n, \mathbf{k}, +}$ in the case of interband pairing [61], e.g. for $\mathcal{G}_{\omega_n, \mathbf{k}} = [i\omega_n - H_{\mathbf{k}}\tau_z - \Delta(\mathbf{k})\tau_x]^{-1}$, we find

$$\frac{\mathcal{G}_{\omega_n, \mathbf{k}} - \mathcal{G}_{-\omega_n, \mathbf{k}}}{2} \simeq -i\omega_n \frac{1}{\omega_n^2 + H_{\mathbf{k}}^2 + \Delta(\mathbf{k})^2} - \omega_n \tau_y \times \frac{1}{\omega_n^2 + H_{\mathbf{k}}^2 + \Delta(\mathbf{k})^2} [H_{\mathbf{k}}, \Delta(\mathbf{k})] \frac{1}{\omega_n^2 + H_{\mathbf{k}}^2 + \Delta(\mathbf{k})^2}. \quad (\text{A8})$$

A frequency independent gap function $\Delta(\mathbf{k})\tau_x$ thus generates an odd frequency anomalous Green's function proportional to τ_y . Analogously to the even frequency case we classify the components of the pair amplitude

$$F_{\omega_n, \mathbf{k}, -} = \sum_{i=0}^8 F_{\omega_n, \mathbf{k}, -}^{(i)} \lambda_i. \quad (\text{A9})$$

The transformation behavior of all components is presented in tables VI and VII, where the former (latter) table is devoted to states which are even (odd) under spatial inversion and odd (even) under transposition in the matrix space of orbitals. We note that, in a purely 2D model, the coefficients of all Gell-Mann matrices but $\lambda_{2,4,6}$ vanish by symmetry.

i	\hat{P}_x	\hat{P}_y	\hat{P}_z	$\hat{R}_{\pi/2}$	examples
2	-	-	+	+	$s_x s_y (c_x - c_y)$
$\begin{pmatrix} 5 \\ 7 \end{pmatrix}$	$\begin{pmatrix} + & 0 \\ 0 & - \end{pmatrix}$	$\begin{pmatrix} - & 0 \\ 0 & + \end{pmatrix}$	$\begin{pmatrix} - & 0 \\ 0 & - \end{pmatrix}$	$\begin{pmatrix} 0 & - \\ + & 0 \end{pmatrix}$	$\begin{pmatrix} s_y s_z \\ s_x s_z \end{pmatrix}$

TABLE VI. Transformation behavior of coefficients $F_{\omega_n, \mathbf{k}, -}^{(i)}$, see Eq. (A9), which are odd under $\omega_n \rightarrow -\omega_n$ and under transposition in orbital space, but even under spatial inversion. The notation is the same as in Table IV.

i	\hat{P}_x	\hat{P}_y	\hat{P}_z	$\hat{R}_{\pi/2}$	examples
0	-	-	-	-	$s_x s_y s_z$
1	+	+	-	+	$s_z, c_{x+y} s_z$
3	-	-	-	+	$s_x s_y s_z (c_x - c_y)$
$\begin{pmatrix} 4 \\ 6 \end{pmatrix}$	$\begin{pmatrix} - & 0 \\ 0 & + \end{pmatrix}$	$\begin{pmatrix} + & 0 \\ 0 & - \end{pmatrix}$	$\begin{pmatrix} + & 0 \\ 0 & + \end{pmatrix}$	$\begin{pmatrix} 0 & + \\ - & 0 \end{pmatrix}$	$\begin{pmatrix} s_x \\ s_y \end{pmatrix}$
8	-	-	-	-	$s_x s_y s_z$

TABLE VII. Transformation behavior of coefficients $F_{\omega_n, \mathbf{k}, -}^{(i)}$, see Eq. (A9), which are odd under $\omega_n \rightarrow -\omega_n$ and $\mathbf{k} \rightarrow -\mathbf{k}$ but even in orbital space. The notation is the same as in Table IV.

4. Gell-Mann matrices

The Gell-Mann Matrices are

$$\lambda_0 = \sqrt{\frac{2}{3}} \mathbf{1},$$

and

$$\begin{aligned} \lambda_1 &= \begin{pmatrix} 0 & 1 & 0 \\ 1 & 0 & 0 \\ 0 & 0 & 0 \end{pmatrix}, \lambda_2 = \begin{pmatrix} 0 & -i & 0 \\ i & 0 & 0 \\ 0 & 0 & 0 \end{pmatrix}, \\ \lambda_3 &= \begin{pmatrix} 1 & 0 & 0 \\ 0 & -1 & 0 \\ 0 & 0 & 0 \end{pmatrix}, \lambda_4 = \begin{pmatrix} 0 & 0 & 1 \\ 0 & 0 & 0 \\ 1 & 0 & 0 \end{pmatrix}, \\ \lambda_5 &= \begin{pmatrix} 0 & 0 & -i \\ 0 & 0 & 0 \\ i & 0 & 0 \end{pmatrix}, \lambda_6 = \begin{pmatrix} 0 & 0 & 0 \\ 0 & 0 & 1 \\ 0 & 1 & 0 \end{pmatrix}, \\ \lambda_7 &= \begin{pmatrix} 0 & 0 & 0 \\ 0 & 0 & -i \\ 0 & i & 0 \end{pmatrix}, \lambda_8 = \frac{1}{\sqrt{3}} \begin{pmatrix} 1 & 0 & 0 \\ 0 & 1 & 0 \\ 0 & 0 & -2 \end{pmatrix}. \end{aligned} \quad (\text{A10})$$

These matrices are a complete basis set of the Lie algebra $\mathfrak{u}(3)$ which are orthonormal under the trace form $\text{tr} \lambda_i \lambda_j = 2\delta_{ij}$.

Appendix B: Generalized t-J model

This appendix includes details on microscopic interactions.

1. Effective interaction in the Cooper channel.

We will consider only the spin singlet channel in which we define

$$(\Psi_{\mathbf{k}}^\dagger)_{mm'} = \frac{1}{2}[c_{\mathbf{k},m,\uparrow}^\dagger c_{-\mathbf{k},m',\downarrow}^\dagger - \uparrow\leftrightarrow\downarrow], \quad (\text{B1a})$$

$$(\Psi_{\mathbf{k}})_{m'm} = \frac{1}{2}[c_{-\mathbf{k},m',\downarrow} c_{\mathbf{k},m,\uparrow} - \uparrow\leftrightarrow\downarrow]. \quad (\text{B1b})$$

$$H_{\text{IA}} \doteq \sum_{mm'} \sum_{\mathbf{k},\mathbf{k}'} V_{\mathbf{k},\mathbf{k}'}^{mm',(S)} (\Psi_{\mathbf{k}}^\dagger)_{(mm')} (\Psi_{\mathbf{k}'})_{(mm')} + \sum_{mm'} \sum_{\mathbf{k},\mathbf{k}'} V_{\mathbf{k},\mathbf{k}'}^{mm',(A)} (\Psi_{\mathbf{k}}^\dagger)_{[mm']} (\Psi_{\mathbf{k}'})_{[m'm]}, \quad (\text{B2a})$$

where the superscripts (S) ((A)) denote symmetry (antisymmetry) under $\mathbf{k} \rightarrow -\mathbf{k}$

$$V_{\mathbf{k},\mathbf{k}'}^{mm',(S)} = \bar{U} + 2J_{\text{H},2}(\delta_{mm'} - 1) - \frac{3J_1^{mm'}}{4}((c_x + c_y)(c_{x'} + c_{y'}) + (c_x - c_y)(c_{x'} - c_{y'})) - \frac{3J_2^{mm'}}{2}(c_x c_y c_{x'} c_{y'} + s_x s_y s_{x'} s_{y'}) \quad (\text{B2b})$$

$$V_{\mathbf{k},\mathbf{k}'}^{mm',(A)} = -\frac{3J_1^{mm'}}{2}(s_x s_{x'} + s_y s_{y'}) - \frac{3J_2^{mm'}}{2}(s_x c_y s_{x'} c_{y'} + c_x s_y c_{x'} s_{y'}), \quad (\text{B2c})$$

where $\bar{U} = U + \frac{3}{2}J_{\text{H},1}$. Assuming s-wave pairing and exploiting the crystal symmetries in Eq. (B2a) we obtain $V_{\mathbf{k},\mathbf{k}'}^{xz,xz} = V_{\mathbf{k},\mathbf{k}'}^{yz,yz}$ and $V_{\mathbf{k},\mathbf{k}'}^{xz,xy} = V_{\mathbf{k},\mathbf{k}'}^{yz,xy}$. In view of the low power of trigonometric functions, we readily see that only short range pairing is induced. We obtain

$$H_{\text{IA}} = \sum_{\mathbf{k},\mathbf{k}'} \sum_{i=0,1,3,5,7,8} V_{\mathbf{k},\mathbf{k}'}^{(i)} \Psi_{\mathbf{k}}^{(i),\dagger} \Psi_{\mathbf{k}'}^{(i)} + \sum_{\mathbf{k},\mathbf{k}'} V_{\mathbf{k},\mathbf{k}'}^{(0,8)} [\Psi_{\mathbf{k}}^{(0),\dagger} \Psi_{\mathbf{k}'}^{(8)} + H.c.], \quad (\text{B3a})$$

where

$$\Psi_{\mathbf{k}}^{(i)} = \sum_{mm'} (\Psi_{\mathbf{k}})_{mm'} [\lambda_i]_{m',m}/2 \quad (\text{B3b})$$

and

$$V_{\mathbf{k},\mathbf{k}'}^{(0)} = 2[2V_{\mathbf{k},\mathbf{k}'}^{xz,xz} + V_{\mathbf{k},\mathbf{k}'}^{xy,xy}]/3 \quad (\text{B3c})$$

$$V_{\mathbf{k},\mathbf{k}'}^{(8)} = 2[2V_{\mathbf{k},\mathbf{k}'}^{xy,xy} + V_{\mathbf{k},\mathbf{k}'}^{xz,xz}]/3 \quad (\text{B3d})$$

$$V_{\mathbf{k},\mathbf{k}'}^{(0,8)} = \sqrt{8}[V_{\mathbf{k},\mathbf{k}'}^{xz,xz} - V_{\mathbf{k},\mathbf{k}'}^{xy,xy}]/3 \quad (\text{B3e})$$

$$V_{\mathbf{k},\mathbf{k}'}^{(3)} = 2V_{\mathbf{k},\mathbf{k}'}^{xz,xz} \quad (\text{B3f})$$

$$V_{\mathbf{k},\mathbf{k}'}^{(1)} = 2V_{\mathbf{k},\mathbf{k}'}^{xz,yz} \quad (\text{B3g})$$

$$V_{\mathbf{k},\mathbf{k}'}^{(5,7)} = 2V_{\mathbf{k},\mathbf{k}'}^{xz,xy}. \quad (\text{B3h})$$

We note that we only need the s-wave part for $i = 0, 8$, d-wave part for $i = 1, 3$ and p-wave part for $i = 5, 7$. Thus Coulomb repulsion only affects channels $i = 0, 8$. This directly leads to the interactions g_C entering the Landau free energy in Eq. (30).

These Cooper pair operators have the property $(\Psi_{\mathbf{k}}^\dagger)_{mm'} = (\Psi_{-\mathbf{k}}^\dagger)_{m'm}$. By means of these operators, Eqs. (3) and (29) lead to the following interactions in the Cooper channel,

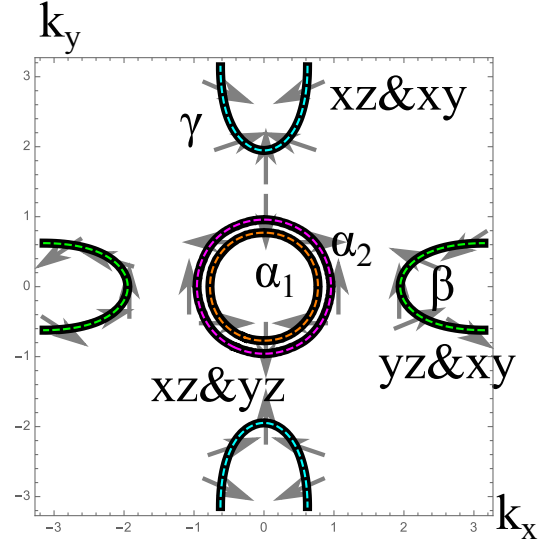


FIG. 6. Fermi surfaces for a three band model based on Ref. [52]. The black curves correspond to the solution of the full matrix Hamiltonian, colored dashed lines correspond to approximate solutions using the projection on the two orbitals indicated by each of the Fermi surfaces. This picture also includes the vectors $\hat{n}^{\alpha,\beta,\gamma}$ which rotate in *different* orbital spaces for different Fermi surfaces.

2. Kinetic term of the generalized t-J model

Without repeating details, we replot the Fermi surfaces as suggested by the three orbital tight binding model [52] in Fig. 6. Motivated by the excellent numerical agreement due to the large separation of bands near the Fermi surface, we only keep two orbitals near each Fermisurface. The projector

on eigenfunctions of the model may then be parameterized by the vectors $\hat{n}^{\alpha,\beta,\gamma}$ which are also plotted in Fig. 6 and account for the rotation of the orbital degrees of freedom around the Fermi surface. Near the two central hole pockets we obtain the projectors on the states in orbital space

$$|u_1^{(0)}\rangle \langle u_1^{(0)}| = \frac{I_{\alpha,0} + \hat{n}_\alpha \mathbf{I}_\alpha}{2} \text{ (inner pocket),} \quad (\text{B4})$$

$$|u_2^{(0)}\rangle \langle u_2^{(0)}| = \frac{I_{\alpha,0} - \hat{n}_\alpha \mathbf{I}_\alpha}{2} \text{ (outer pocket),} \quad (\text{B5})$$

where $\mathbf{I}^\alpha = (\lambda_1, \lambda_2, \lambda_3)$ is the set of Pauli matrices in the space of xz and yz orbitals and $I_{\alpha,0}$ is unity in this space. At the electron pocket β , the projector on the band at the Fermi surface is

$$|u_3^{(0)}\rangle \langle u_3^{(0)}| = \frac{I_{\beta,0} - \hat{n}^\beta \mathbf{I}_\beta}{2} \quad (\text{B6})$$

where $\mathbf{I}^\beta = (\lambda_6, \lambda_7, \frac{-\lambda_3 + \sqrt{3}\lambda_8}{2})$ is the set of Pauli matrices in the space of yz and xy orbitals and $I_{\beta,0}$ is unity in this space. An analogous term may be obtained at the γ pocket by a $\pi/2$ rotation, we do not report it here.

We consider a simpler model than Fig. 6, assuming circular Fermi surfaces at Γ, X, Y which are parametrized by an angle θ and $\hat{n}^\alpha = (2c_\theta s_\theta, c_\theta^2 - s_\theta^2)^T$ in the space $(|xz\rangle, |yz\rangle)^T$ for the central hole pockets. Furthermore, we assume $\langle \hat{n}_z^\beta \rangle_{FS\beta} = 1/2, \langle (\hat{n}_z^\beta)^2 \rangle_{FS\beta} = 1/3$. This is approximately the same result as one would obtain by a simple ansatz $\hat{n}^\beta = (-2s_\theta, c_\theta^2)^T / (1 + s_\theta^2)$ in the space $(|yz\rangle, |xy\rangle)^T$ which is qualitatively in agreement with the orbital structure in Fig. 6. We approximate $c_x c_y \approx \pm 1$ on hole/electron pockets and $s_x s_y \rightarrow k_{F,h}^2 s_\theta c_\theta$ on the hole pockets, $c_x - c_y \rightarrow k_{F,h}^2 (s_\theta^2 - c_\theta^2)/2$ on the hole pockets and $c_x - c_y = -2$ on the electron pocket. We set $k_{F,h} = \sqrt{2/3}$. Then the susceptibility matrix

$$\chi_{\Gamma\Gamma'} = \frac{1}{2} \sum_{n,\mathbf{k}} (\varphi^\Gamma(\mathbf{k}) \lambda_{i(\Gamma)})_{nn} (\varphi^{\Gamma'}(\mathbf{k}) \lambda_{i(\Gamma')})_{nn} \frac{\tanh(\frac{\epsilon_n}{2T})}{\epsilon_n} \\ \simeq \ln(\Lambda/T) [\rho_{h_1} \tilde{\chi}^{(h_1)} + \rho_{h_2} \tilde{\chi}^{(h_2)} + 2\rho_e \tilde{\chi}^{(e)}]_{\Gamma\Gamma'}. \quad (\text{B7})$$

is determined by the following matrices in the space of

$\Delta_{\Gamma=1\dots 5}$

$$\frac{\tilde{\chi}^{(h_1)} + \tilde{\chi}^{(h_2)}}{2} = \begin{pmatrix} \frac{2}{3} & \frac{\sqrt{2}}{3} & \frac{2}{3} & 0 & 0 \\ \frac{\sqrt{2}}{3} & \frac{1}{3} & \frac{\sqrt{2}}{3} & 0 & 0 \\ \frac{2}{3} & \frac{\sqrt{2}}{3} & \frac{2}{3} & 0 & 0 \\ 0 & 0 & 0 & \frac{1}{8} & -\frac{1}{24} \\ 0 & 0 & 0 & -\frac{1}{24} & \frac{1}{8} \end{pmatrix}, \quad (\text{B8})$$

$$\tilde{\chi}^{(e)} = \begin{pmatrix} \frac{2}{3} & -\frac{5}{6\sqrt{2}} & -\frac{2}{3} & 0 & \frac{1}{\sqrt{6}} \\ -\frac{5}{6\sqrt{2}} & \frac{7}{12} & \frac{5}{6\sqrt{2}} & 0 & -\frac{1}{2\sqrt{3}} \\ -\frac{2}{3} & \frac{5}{6\sqrt{2}} & \frac{2}{3} & 0 & -\frac{1}{\sqrt{6}} \\ 0 & 0 & 0 & 0 & 0 \\ \frac{1}{\sqrt{6}} & -\frac{1}{2\sqrt{3}} & -\frac{1}{\sqrt{6}} & 0 & \frac{1}{3} \end{pmatrix}. \quad (\text{B9})$$

For simplicity we assume $\rho_{h_1} = \rho_{h_2} \equiv \rho_h$ in Fig. 4 and we use the kernel of the matrix in the quadratic part of Eq. (12) to determine T_c at finite \bar{U} .

3. Renormalization group for the two band model

In this appendix, we briefly recapitulate the RG treatment of a two-band model [14]. Following the discussion of the previous appendix, the Cooper pair creation operator in a given band n takes the form

$$[\Psi_n^{(i)}]^\dagger = \frac{1}{2} \sum_{\mathbf{k}} \{c_{\mathbf{k},\uparrow,n}^\dagger c_{-\mathbf{k},\downarrow,n}^\dagger - \uparrow\leftrightarrow\downarrow\} (u_{\mathbf{k},n}^\dagger \lambda_i u_{\mathbf{k},n}). \quad (\text{B10})$$

Here we used that $u_{-k,n}^* = u_{k,n}$. For the two band case the situation simplifies as $(u_{\mathbf{k},n}^\dagger \lambda_i u_{\mathbf{k},n}) \rightarrow 1$. In band space, Cooper interactions take the form

$$H_{\text{int}} = \Psi_n^\dagger G_{nn'} \Psi_{n'}. \quad (\text{B11})$$

As mentioned, for pure Coulomb interaction, $G_{nn'} \propto U$ (independently of n, n'). Clearly, the ladder RG describing only particle-particle logarithms (assuming non-degenerate bands) leads to

$$\frac{dG_{nn'}}{d \ln(D/T)} = - \sum_{n''} G_{nn''} \rho_{n''} G_{n''n'}. \quad (\text{B12})$$

These equations for three separate coupling constants imply the Eqs. (8) along with one conserved coupling constant

$$\frac{d}{d \ln(D/T)} \left(\frac{G_{11}\rho_1 - G_{22}\rho_2}{G_{12}\sqrt{\rho_1\rho_2}} \right) = 0. \quad (\text{B13})$$

[1] Y. Kamihara, T. Watanabe, M. Hirano, and H. Hosono, Journal of the American Chemical Society **130**, 3296 (2008).

[2] H. Takahashi, A. Sugimoto, Y. Nambu, T. Yamauchi, Y. Hi-

rata, T. Kawakami, M. Avdeev, K. Matsubayashi, F. Du, C. Kawashima, H. Soeda, S. Nakano, Y. Uwatoko, Y. Ueda, T. J. Sato, and K. Ohgushi, Nat Mater **14**, 1008 (2015).

- [3] Phys. Rev. Lett. **115**, 246402 (2015).
- [4] D. Huang and J. E. Hoffman, Annual Review of Condensed Matter Physics **8**, 311 (2017).
- [5] T. Sato, K. Nakayama, Y. Sekiba, P. Richard, Y.-M. Xu, S. Souma, T. Takahashi, G. F. Chen, J. L. Luo, N. L. Wang, and H. Ding, Phys. Rev. Lett. **103**, 047002 (2009).
- [6] T. Yoshida, I. Nishi, A. Fujimori, M. Yi, R. Moore, D.-H. Lu, Z.-X. Shen, K. Kihou, P. Shirage, H. Kito, C. Lee, A. Iyo, H. Eisaki, and H. Harima, Journal of Physics and Chemistry of Solids **72**, 465 (2011), spectroscopies in Novel Superconductors 2010.
- [7] C. C. Chang, T. K. Chen, W. C. Lee, P. H. Lin, M. J. Wang, Y. C. Wen, P. M. Wu, and M. K. Wu, Physica C: Superconductivity and its Applications **514**, 423 (2015).
- [8] T.-H. Lee, A. Chubukov, H. Miao, and G. Kotliar, Phys. Rev. Lett. **121**, 187003 (2018).
- [9] T. Miyake, K. Nakamura, R. Arita, and M. Imada, Journal of the Physical Society of Japan **79**, 044705 (2010).
- [10] M. D. Watson, S. Backes, A. A. Haghighirad, M. Hoesch, T. K. Kim, A. I. Coldea, and R. Valentí, Phys. Rev. B **95**, 081106 (2017).
- [11] D. Evtushinsky, M. Aichhorn, Y. Sassa, Z.-H. Liu, J. Maletz, T. Wolf, A. Yaresko, S. Biermann, S. Borisenko, and B. Buchner, arXiv preprint arXiv:1612.02313 (2016).
- [12] L. deMedici, in *Iron-Based Superconductivity* (Springer, 2015) pp. 409–441.
- [13] Q. Si, R. Yu, and E. Abrahams, Nature Reviews Materials **1**, 1 (2016).
- [14] A. Chubukov, in *Iron-Based Superconductivity* (Springer, 2015) pp. 255–329.
- [15] R. M. Fernandes and A. V. Chubukov, Reports on Progress in Physics **80**, 014503 (2016).
- [16] P. J. Hirschfeld, Comptes Rendus Physique **17**, 197 (2016).
- [17] Y. Bang and G. R. Stewart, Journal of Physics: Condensed Matter **29**, 123003 (2017).
- [18] F. Hardy, A. E. Böhmer, D. Aoki, P. Burger, T. Wolf, P. Schweiss, R. Heid, P. Adelman, Y. X. Yao, G. Kotliar, J. Schmalian, and C. Meingast, Phys. Rev. Lett. **111**, 027002 (2013).
- [19] M. Yi, Z.-K. Liu, Y. Zhang, R. Yu, J. X. Zhu, J. J. Lee, R. G. Moore, F. T. Schmitt, W. Li, S. C. Riggs, J. H. Chu, B. Lv, J. Hu, M. Hashimoto, S. K. Mo, Z. Hussain, Z. Q. Mao, C. W. Chu, I. R. Fisher, Q. Si, Z. X. Shen, and D. H. Lu, Nat. Comm. **6**, 7777 (2015).
- [20] P. O. Sprau, A. Kostin, A. Kreisel, A. E. Böhmer, V. Taufour, P. C. Canfield, S. Mukherjee, P. J. Hirschfeld, B. M. Andersen, and J. C. S. Davis, Science **357**, 75 (2017).
- [21] In a 5 orbital model there are five adjustable parameters, one for each pair angular momentum $L \in [0, 4]$. However in a simplified 3 orbital model, the pseudo angular momentum of the electrons is $l = 1$, leading to a total $L \in [0, 2]$, giving rise to three interaction parameters, allowing the simplified interaction Hamiltonian listed here..
- [22] W. L. McMillan, Phys. Rev. **167**, 331 (1968).
- [23] N. Bogolyubov, V. Tolmachev, and D. Shirkov, *Noviy metod v teorii sverkhprovodimosti* (Izdatel'stvo akademii nauk SSSR, Moscow, 1958) [Engl. transl. "A new method in the theory of superconductivity", Consultants Bureau, New York, 1959.].
- [24] A. I. Coldea, J. D. Fletcher, A. Carrington, J. G. Analytis, A. F. Bangura, J.-H. Chu, A. S. Erickson, I. R. Fisher, N. E. Hussey, and R. D. McDonald, Phys. Rev. Lett. **101**, 216402 (2008).
- [25] D. V. Evtushinsky, D. S. Inosov, V. B. Zabolotnyy, A. Koitzsch, M. Knupfer, B. Büchner, M. S. Viazovska, G. L. Sun, V. Hinkov, A. V. Boris, C. T. Lin, B. Keimer, A. Varykhalov, A. A. Kordyuk, and S. V. Borisenko, Phys. Rev. B **79**, 054517 (2009).
- [26] H. Ding, K. Nakayama, P. Richard, S. Souma, T. Sato, T. Takahashi, M. Neupane, Y. Xu, Z. Pan, A. Fedorov, et al., Journal of Physics: Condensed Matter **23**, 135701 (2011).
- [27] C. Liu, T. Kondo, R. M. Fernandes, A. D. Palczewski, E. D. Mun, N. Ni, A. N. Thaler, A. Bostwick, E. Rotenberg, J. Schmalian, et al., Nature Physics **6**, 419 (2010).
- [28] C. Liu, A. D. Palczewski, R. S. Dhaka, T. Kondo, R. M. Fernandes, E. D. Mun, H. Hodovanets, A. N. Thaler, J. Schmalian, S. L. Bud'ko, P. C. Canfield, and A. Kaminski, Phys. Rev. B **84**, 020509 (2011).
- [29] A. Tamai, A. Y. Ganin, E. Rozbicki, J. Bacsá, W. Meevasana, P. D. C. King, M. Caffio, R. Schaub, S. Margadonna, K. Prasad, M. J. Rosseinsky, and F. Baumberger, Phys. Rev. Lett. **104**, 097002 (2010).
- [30] Z. K. Liu, M. Yi, Y. Zhang, J. Hu, R. Yu, J. X. Zhu, R. H. He, Y. L. Chen, M. Hashimoto, R. G. Moore, S. K. Mo, Z. Hussain, Q. Si, Z. Q. Mao, D. H. Lu, and Z. X. Shen, Phys. Rev. B **92**, 235138 (2015).
- [31] T. Qian, X.-P. Wang, W.-C. Jin, P. Zhang, P. Richard, G. Xu, X. Dai, Z. Fang, J.-G. Guo, X.-L. Chen, and H. Ding, Phys. Rev. Lett. **106**, 187001 (2011).
- [32] S. He, J. He, W. Zhang, L. Zhao, D. Liu, X. Liu, D. Mou, Y.-B. Ou, Q.-Y. Wang, Z. Li, et al., Nature materials **12**, 605 (2013).
- [33] S. Maiti and A. V. Chubukov, Phys. Rev. B **82**, 214515 (2010).
- [34] A. V. Chubukov, M. Khodas, and R. M. Fernandes, Phys. Rev. X **6**, 041045 (2016).
- [35] R. Thomale, C. Platt, J. Hu, C. Honerkamp, and B. A. Bernevig, Phys. Rev. B **80**, 180505 (2009).
- [36] E. König, A. M. Tsvelik, and P. Coleman, arXiv:1802.10579 (2018).
- [37] Z. Yin, K. Haule, and G. Kotliar, Nature Physics **10**, 845 (2014).
- [38] A. V. Chubukov, O. Vafek, and R. M. Fernandes, Phys. Rev. B **94**, 174518 (2016).
- [39] E. M. Nica, R. Yu, and Q. Si, npj Quantum Materials, 1 (2017).
- [40] Y. Gao, W. P. Su, and J. X. Zhu, Phys. Rev. B **81**, 104504 (2010).
- [41] T. T. Ong and P. Coleman, Phys. Rev. Lett. **111**, 217003 (2013).
- [42] T. Ong, P. Coleman, and J. Schmalian, PNAS **113**, 5486 (2016).
- [43] R. Nourafkan, G. Kotliar, and A.-M. Tremblay, Physical review letters **117**, 137001 (2016).
- [44] Y. Wang, T. Berlijn, P. J. Hirschfeld, D. J. Scalapino, and T. A. Maier, Phys. Rev. Lett. **114**, 107002 (2015).
- [45] X. Dai, Z. Fang, Y. Zhou, and F.-C. Zhang, Phys. Rev. Lett. **101**, 057008 (2008).
- [46] Z. F. Weng, J. L. Zhang, M. Smidman, T. Shang, J. Quintanilla, J. F. Annett, M. Nicklas, G. M. Pang, L. Jiao, W. B. Jiang, Y. Chen, F. Steglich, and H. Q. Yuan, Phys. Rev. Lett. **117**, 027001 (2016).
- [47] I. I. Mazin, D. J. Singh, M. D. Johannes, and M. H. Du, Phys. Rev. Lett. **101**, 057003 (2008).
- [48] P.J. Hirschfeld, M.M. Korshunov, I.I. Mazin, Rep. Prog. Phys. **74**, 124508 (2011).
- [49] Y. Bang, New J. Phys. **16**, 023029 (2014).
- [50] M. H. Fischer, New Journal of Physics **15**, 073006 (2013).
- [51] J. Linder and A. V. Balatsky, (2017), arXiv:1709.03986 [cond-mat.supr-con].
- [52] M. Daghofer, A. Nicholson, A. Moreo, and E. Dagotto, Physical Review B **81**, 014511 (2010).
- [53] S. Maiti and A. V. Chubukov, Phys. Rev. B **87**, 144511 (2013).
- [54] If the lowest eigenvalue was not degenerate, one would be

forced to require the eigenvector \hat{e} to change along with χ_{IC}, χ_{IIC} as the electronic structure alters. Such a mechanism is unknown and, in any case, different from the proposed orbital and k-space flexibility.

- [55] M. Khodas and A. V. Chubukov, Physical Review Letters **108**, 247003 (2012).
- [56] D. F. Agterberg, T. Shishidou, J. O'Halloran, P. M. R. Brydon, and M. Weinert, Phys. Rev. Lett. **119**, 267001 (2017).
- [57] P. A. Lee and X.-G. Wen, Physical Review B **78**, 144517 (2008).
- [58] O. Vafek and A. V. Chubukov, Physical Review Letters **118**, 087003 (2017).
- [59] A.K.C. Cheung and D.F. Agterberg, arXiv preprint arXiv:1809.10714 (2018).
- [60] D. Vollhardt and P. Woelfle, The Superfluid Phases Of Helium 3 (Taylor & Francis, 1990).
- [61] A. M. Black-Schaffer and A. V. Balatsky, Phys. Rev. B **88**, 104514 (2013).